A HYBRID DATA-DRIVEN APPROACH FOR PREDICTING RETAINING WALL DEFORMATION

L. L. Mu & K. Yan.

Department of Geotechnical Engineering, Tongji University, Shanghai 200092, China

Key Laboratory of Geotechnical and Underground Engineering of Ministry of Education, Tongji University, Shanghai 200092, China

ABSTRACT: Predicting retaining wall deformation induced by excavation is a significant challenge in geotechnical engineering, complicated by complex soil-structure interactions and inherent subsurface uncertainties. A primary obstacle for data-driven models is the reliance on large-scale training datasets; however, field-measured data from engineering projects are often sparse and noisy, hindering the development of high-precision predictive models. To overcome these limitations, this study introduces an innovative hybrid data-driven approach, integrating a massive synthetic dataset from 87,368 Finite Element (FE) simulations with 3,005 measured data points from 18 case histories. A comparative analysis was conducted by developing three separate Backpropagation Neural Network (BPNN) models trained on the FE data alone, the case history data alone, and the proposed hybrid database. The results demonstrate the superior performance of the model trained on the hybrid database, which achieved a prediction accuracy where 96.8% of absolute errors were less than 2 mm and 100% of relative errors were less than 5% on a combined test set. Furthermore, validation against an independent, real-world engineering project confirmed that prediction errors were predominantly below 2 mm. This study confirms that augmenting sparse field measurements with high-fidelity numerical data is an effective strategy for developing robust and reliable machine learning models for geotechnical applications.

1. INTRODUCTION

Ongoing urbanization and the intensifying scarcity of urban land have spurred the development of underground space, leading to increasingly large and deep foundation pit excavations. In dense urban environments, such excavations are frequently in close proximity to existing buildings and critical underground utilities. Deformation of the retaining system induced by excavation can trigger ground movement, posing risks to adjacent structures and infrastructure, thereby jeopardizing both the stability of the excavation and the integrity of the surrounding environment (Seo and Chung, 2023; Bovolenta and Antonio, 2021). Consequently, the ability to accurately predict and control excavation-induced wall deformation remains a critical and long-standing objective in geotechnical engineering.

Traditional prediction methods encompass empirical approaches from field data correlations (Mana and Clough, 1981; Ou and Tang, 1994; Kung et al., 2007; Goh et al., 2017), theoretical calculations rooted in soil and structural mechanics (Peck, 1969; Hsieh and Ou, 1998; Xu and Poulos, 2000; Zhang et al., 2011), and the Finite Element Method (FEM), which facilitates detailed parametric analysis (Clough and Duncan, 1971; Borja and Ronaldo, 1990; Li et al., 2021). While convenient, empirical methods often neglect crucial construction factors (Finno and Calvello, 2005), and theoretical methods depend on simplifying assumptions that can diverge significantly from field conditions (Cao et al., 2014). Although FEM overcomes some of these limitations, its numerical simulations are complex and computationally intensive (Mu et al., 2020). Crucially, the fidelity of FEM predictions is highly contingent upon the chosen constitutive models and input parameters, which may not adequately capture the multifaceted nature of real-world soil behaviours and construction processes.

For complex excavations characterized by significant uncertainty and non-linearity, traditional methods often fail to account for all influencing factors comprehensively (Jamali et al., 2013), limiting their utility for dynamic, in-construction prediction. The demand for stringent deformation control thus necessitates more intelligent and responsive predictive approaches. Artificial Neural Networks (ANNs), particularly the Backpropagation Neural Network (BPNN), have demonstrated considerable promise for such non-linear, multi-variable geotechnical problems due to their powerful learning and generalization capabilities (Hu et al., 2013). ANNs offer distinct

advantages, notably faster computation times compared to traditional methods (Goh et al., 1995). For instance, Goh et al. (1995) utilized a BPNN to learn from FEM results, achieving reasonable predictions for wall deformations in clay. However, the limited input parameters (especially soil properties) in their study impeded the creation of robust mapping relationships applicable across diverse soil profiles and construction scenarios (Gao et al., 2002). The performance of a BPNN is fundamentally linked to the volume and quality of its training data (Yuan et al., 2000; Hu et al., 2013). Unfortunately, field monitoring data is often incomplete or unreliable due to equipment malfunctions and operational errors, making the acquisition of a large, high-quality dataset a formidable challenge. While many researchers have combined BPNN with other intelligent algorithms to enhance its predictive power (Ma et al., 2008; Cao et al., 2014; Zhang et al., 2020; Cui et al., 2021), these hybrid models have primarily focused on reducing training set size and computation time, often without adequately considering the holistic impact of soil conditions, retaining structure parameters, and construction sequences.

To address this critical data challenge, this paper introduces a novel data-centric strategy centered on a hybrid sample database. The core idea is to synergistically combine the strengths of FE simulation data and measured case history data. This leverages the high volume, parametric control, and broad coverage of FE simulations while incorporating the real-world complexities and constraints captured by field monitoring data. Such an approach is designed to overcome the limitations inherent in using either data source in isolation. To validate this strategy, we developed a comprehensive BPNN model incorporating inputs that reflect soil small-strain properties, foundation pit geometry, and retaining structure parameters. A large-scale FE database was generated via automated PLAXIS simulations, and a case history database was compiled from monitored projects in Shanghai. These datasets were integrated to form the hybrid database. The BPNN model was then trained on this hybrid database, and its performance was systematically benchmarked against models trained solely on FE data and solely on field data. The model's predictive capability was verified against FE test cases.

2. METHODOLOGY

2.1 BACKPROPAGATION NEURAL NETWORK (BPNN)

The deformation of a retaining wall is influenced by a multitude of complex factors with varying degrees of impact and intricate interactions between the structure and the surrounding geological environment. Previous studies employing BPNN have often utilized a limited set of input parameters, focusing primarily on basic soil properties. This narrow scope is insufficient for establishing a comprehensive mapping relationship that accounts for diverse soil profiles and construction conditions. Therefore, this work adopts a more holistic approach by selecting input parameters that encompass soil properties reflecting small-strain characteristics, foundation pit geometry, and retaining structure parameters. This comprehensive input set enables the BPNN model to effectively capture the influence of individual soil layer characteristics, the location and mechanics of support systems, and excavation conditions on the maximum retaining wall deformation. The schematic diagram of its BPNN structure is shown in Figure 1.

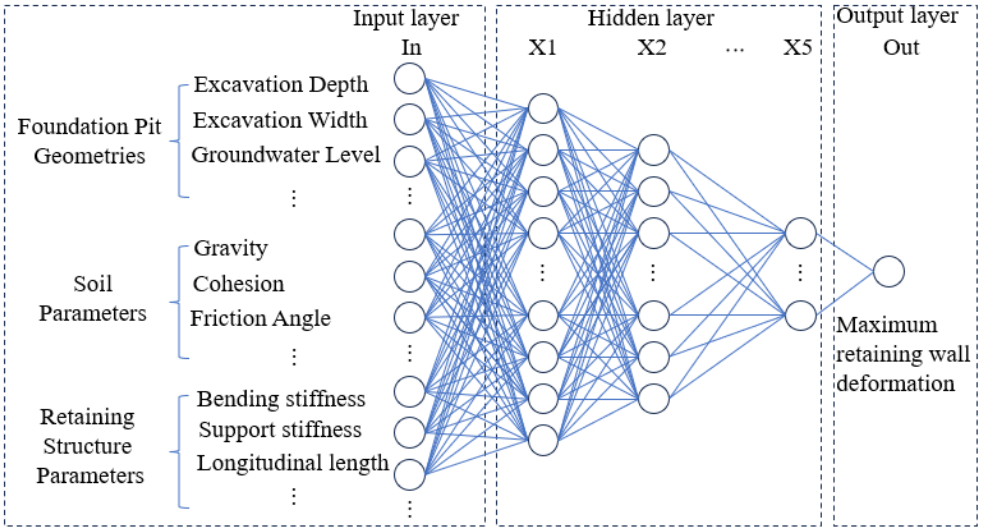

Figure 1: Schematic diagram of the internal structure of BPNN

Accurate prediction of excavation-induced deformation requires capturing small-strain soil behavior. The Hardening Soil Small-strain (HSS) model (Benz, 2007) has been widely demonstrated to reproduce such small-strain behavior relevant to deep excavation simulations (Burland, 1989; Whittle et al., 1994; Kung et al., 2007; Clayton, 2011). Accordingly, five HSS parameters were selected: the reference secant modulus (E_{50}^{ref}), the reference unloading-reloading modulus (E_{ur}^{ref}), the reference tangent modulus for oedometer loading (E_{oed}^{ref}), the initial shear modulus (G_0^{ref}), and the shear strain at which the shear modulus has degraded to 70% ($\gamma_{0.7}$). These were supplemented by four conventional parameters: unit weight (γ), layer thickness (h), effective cohesion (c'), and effective friction angle (φ'), resulting in nine parameters per soil layer.

Excavation geometry significantly impacts lateral wall deformation (Zeng et al., 2019; Ren et al., 2024); thus, excavation depth, excavation width, and groundwater depth were included as input variables. Furthermore, structural characteristics are critical, as the lateral deformation of the retaining wall is a function of its bending stiffness (EI) and embedment depth (Lei and Gong, 2021). Support systems also exert significant influence; thus, the study incorporates key parameters for both the retaining wall and its supports. For the supports, axial stiffness (EA), transverse spacing, design axial force, and vertical spacing from the top of the wall were considered. For the retaining wall, bending stiffness (EI) and total length were selected. A summary of all adopted parameters is provided in **Chyba! Nenalezen zdroj odkazů.**.

Table 1: List of soil and structural parameters

Soil parameters	Enclosure structure and other parameters
Thickness h	Stiffness EA
Unit weight γ	Lateral spacing between support
effective cohesion c'	Distance from supports to top surface
effective friction angle φ'	support axial force
reference secant modulus E_{50}^{ref}	Bending stiffness EI
loading-unloading modulus E_{ur}^{ref}	Longitudinal length
reference tangent modulus in consolidation test E_{oed}^{ref}	Excavation depth
initial shear modulus G_0^{ref}	Excavation width
shear strain $\gamma_{0.7}$	Groundwater depth

2.2 DATABASE

The predictive performance of BPNN models is fundamentally determined by the completeness and quality of training data. However, as discussed earlier, real-world monitoring data is inherently sparse and noisy. Many existing models emphasize algorithmic optimization to reduce dataset size and training effort, often at the expense of ignoring the complex interplay between soil conditions, structural parameters, and construction processes. In contrast, this work adopts a data-centric framework, developing and comparing BPNN models trained on: 1) a large-scale finite element database, 2) a real-world engineering monitoring dataset, and 3) a novel hybrid database combining both. This comparative framework provides direct quantitative evidence that hybrid data fusion leads to enhanced prediction accuracy and robustness.

2.2.1 Finite element modelling

To create the numerical dataset, PLAXIS 2D was employed to generate a comprehensive finite element sample library. This library underpins the development of a predictive model for maximum horizontal wall deformation with robust generalization capabilities. The model is designed to incorporate key variables, including excavation depth and the number of support levels across various construction scenarios, thereby facilitating accurate estimations of maximum horizontal retaining wall deformation.

To generate a substantial and diverse finite element (FE) database, we developed an automated modelling program using the Python scripting interface for PLAXIS 2D. This program enabled batch processing and ensured that parameter values and excavation conditions for each simulation were uncorrelated. The script automated several key processes: generation of soil and structural models,

assignment of material properties, definition of groundwater conditions, mesh generation, and execution of excavation sequences. Critically, it also automatically extracted and recorded the maximum horizontal deformation of the retaining wall and all corresponding input parameters into the database for each simulation.

The parameter values for the FE samples were randomly selected from within the fluctuation ranges observed in the real-world engineering cases compiled for this study. After executing 87,368 individual simulations, the final FE database was established. This dataset, referred to as dataset A, comprises 102 input parameters and one output parameter (maximum horizontal wall deformation), with the specific parameter ranges detailed in Tables 2, 3, 4, and 5.

Table 1 Ranges of soil parameters (Part 1) for the finite element simulation dataset

Soil layer	h (m)	γ (kN/m^3)	c' (kPa)	φ' (°)
1	(1.6,7)	(18.3,19.3)	(19,29)	(13,33)
2	(2.9,10)	(17.4,18.9)	(11,21)	(16.5,32)
3	(3.3,10.8)	(16.7,18.8)	(4,18)	(11,35)
4	(7,19.5)	(16.9,19.4)	(13,17)	(10.5,32.5)
5	(4.6,11.9)	(17.7,19.6)	(16,44)	(12,27.5)
6	(3.5,16.7)	(18.1,19.7)	(17,49)	(18.5,34)
7	(2.5,21.7)	(18.7,20)	(4,50)	(15.5,35.5)
8	(5,27.47)	(18,19.6)	(2,30)	(15.5,35)
9	(20,24)	(18.3,20)	(2,40)	(19,35.5)

Table 2 Ranges of soil parameters (Part 2) for the finite element simulation dataset

Soil layer	E_{50}^{ref} (MPa)	E_{oed}^{ref} (MPa)	E_{ur}^{ref} (MPa)	$\gamma_{0.7}$ (10^{-4})	G_0^{ref} (MPa)
1	(3.78,11.54)	(3.03,9.23)	(23.07,55.37)	(3.2,4.1)	(69.6,129.4)
2	(3.30,14.60)	(2.67,11.71)	(21.18,68.27)	(3.2,4.1)	(51.2,99.3)
3	(3.55,11.77)	(2.84,9.42)	(22.1,56.34)	(3.2,4.1)	(37.8,123.7)
4	(3.55,10.57)	(2.84,8.46)	(22.1,51.34)	(3.2,4.1)	(41,160)
5	(3.31,7.27)	(2.65,5.82)	(21.1,37.6)	(3.2,4.1)	(57.4,123.1)
6	(4.57,11.03)	(3.65,8.82)	(26.35,53.23)	(3.2,4.1)	(70.7,128.4)
7	(6.42,14.09)	(5.14,11.27)	(34.04,66)	(3.2,4.1)	(127.5,176.4)
8	(4.15,14.95)	(3.32,11.96)	(24.6,69.6)	(3.2,4.1)	(64.9,183.9)
9	(5.11,14.71)	(4.09,11.77)	(28.6,68.6)	(3.2,4.1)	(72.8,155.8)

Table 3 Ranges of excavation characteristics for the finite element simulation dataset

Excavation depth (m)	Excavation width (m)	groundwater depth (m)	Bending stiffness EI (GPa · m^2)	Longitudinal length (m)
(0,23)	(50,336)	(1.6,3.5)	(0.38,5.29)	(10,55)

Table 4 Ranges of parameters for the support system in the finite element simulation dataset

Support	Stiffness EA(GN)	Lateral spacing between supports (m)	Distance from supports to top surface (m)
First support	(19.85,35.5)	(6,10)	(0.5,1.5)
Second support	(20,35.5)	(6,10)	(3.2,6.9)
Third support	(20.1,35.5)	(6,10)	(7.1,10.5)
Fourth support	(20.1,35.5)	(6,10)	(11.5,17.4)

2.2.2 Engineering field measurements

To complement the numerical dataset, a comprehensive field database was compiled from real-world engineering projects. Typically, prior to excavation, multiple monitoring points are installed along the perimeter of a foundation pit, generating daily data throughout the construction process. This study collected and organized monitoring data spanning the entire excavation phase, from initial ground breaking to the completion of the base slab. Data was sourced from 18 deep excavation projects in

Shanghai, yielding a total of 3,005 data samples, each corresponding to a measured maximum horizontal deformation of the retaining wall.

Assembling the engineering case database required collecting several key documents for each project: the geotechnical investigation report, which includes statistical tables of soil properties; the design and construction drawings for the excavation; and all relevant construction monitoring data, such as inclinometer reports, support axial force records, and groundwater level observations. A significant challenge was that HSS model parameters, specifically E_{50}^{ref}, E_{ur}^{ref}, E_{oed}^{ref}, G_0^{ref} and $\gamma_{0.7}$, are not directly available from standard site investigation reports. To address this, we adopted the empirical conversion methods proposed by Gu (2021), which derive these HSS parameters from more commonly available data like the void ratio (e) and the compression modulus (Es). The specific conversion relationships used are detailed in Table 6.

Table 5 Empirical conversion used for HSS parameters

Parameter	Empirical method
E_{oed}^{ref}	Clay: E_{oed}^{ref}= -4.34ln(*e*)+3.51 MPa (Based on laboratory test) E_{oed}^{ref}=0.81$E_{s1\text{-}2}$ (Both clay and sandy soil)
E_{50}^{ref}	Clay: E_{50}^{ref}= -5.33ln(*e*)+3.95 MPa (Based on laboratory test) E_{50}^{ref}=1.02$E_{s1\text{-}2}$ (According to this formula if there is no test data for sandy soil)
E_{ur}^{ref}	Clay: E_{ur}^{ref}= -28.8ln(*e*)+24.5 MPa (Based on laboratory test) E_{ur}^{ref}= 4.2$E_{s1\text{-}2}$+7.24 (According to this formula if there is no test data for sandy soil)
G_0^{ref}	Clay (Clayey silt): G_0^{ref}=67.5$e^{-1.57}$ MPa (Based on on-site wave velocity test data) Sandy soil (Sandy silt): G_0^{ref}=98.9$e^{-0.45}$ MPa (Based on on-site wave velocity test data)
$\gamma_{0.7}$	Clay (Clayey silt): $\gamma_{0.7}$=2.4~4.4×10^{-4} the mean value is 3.2×10^{-4} (Based on laboratory test) Sandy soil (Sandy silt)：$\gamma_{0.7}$=2.9~5.2×10^{-4} the mean value is 3.9×10^{-4}(Based on laboratory test)

* *e* is pore ratio; I_p is plasticity index.

2.2.3 Error evaluation

This study aims to develop a high-performance predictive model for retaining wall displacement through a systematic evaluation of various datasets. A Backpropagation Neural Network (BPNN) was employed, configured with 102 input neurons, five fully connected hidden layers with neuron counts of [97, 85, 65, 45, 25] respectively, and a single output neuron. The network utilized the Rectified Linear Unit (ReLU) as its activation function, Mean Squared Error (MSE) as the loss function, and the Adam optimizer with a learning rate of 0.001. To quantitatively assess the performance hierarchy across different datasets, a rigorous 10-fold cross-validation was conducted, with the evaluation metrics summarized in Table 7.

Table 7. Evaluation Metrics Summarized

Evaluation Parameters	Engineering Data	Finite element data	Fusion data
MSE	24.4999 ± 4.6688	25.9283 ± 2.3783	26.3446 ± 2.6525
RMSE	4.9272 ± 0.4717mm	5.0865 ± 0.2352mm	5.1263 ± 0.2565 mm
MAE	3.2070 ± 0.1962mm	3.2965 ± 0.0993mm	3.3364 ± 0.1088 mm
R^2	0.8338 ± 0.0398	0.9830 ± 0.0016	0.9824 ± 0.0016

As illustrated in Fig. 2 and Fig. 3, the model trained on the Engineering dataset exhibits a relatively disperse residual distribution. Although the points are generally centered around the zero-error line, their wide scatter and the "short and wide" shape of the residual histogram reflect the inherent noise and complexity of real-world data. This is consistent with the model's Coefficient of Determination (R^2) of 0.8321 ± 0.0379, indicating an inability to perfectly fit all uncertain field cases. Furthermore, the validation loss in its loss-epoch curve shows significant volatility and large oscillations throughout the training process. While the overall trend is downward, the process is highly unstable, which is a typical behavior when training on a small dataset with high heterogeneity. The optimizer is constantly perturbed by anomalous samples, causing it to oscillate within the loss landscape.

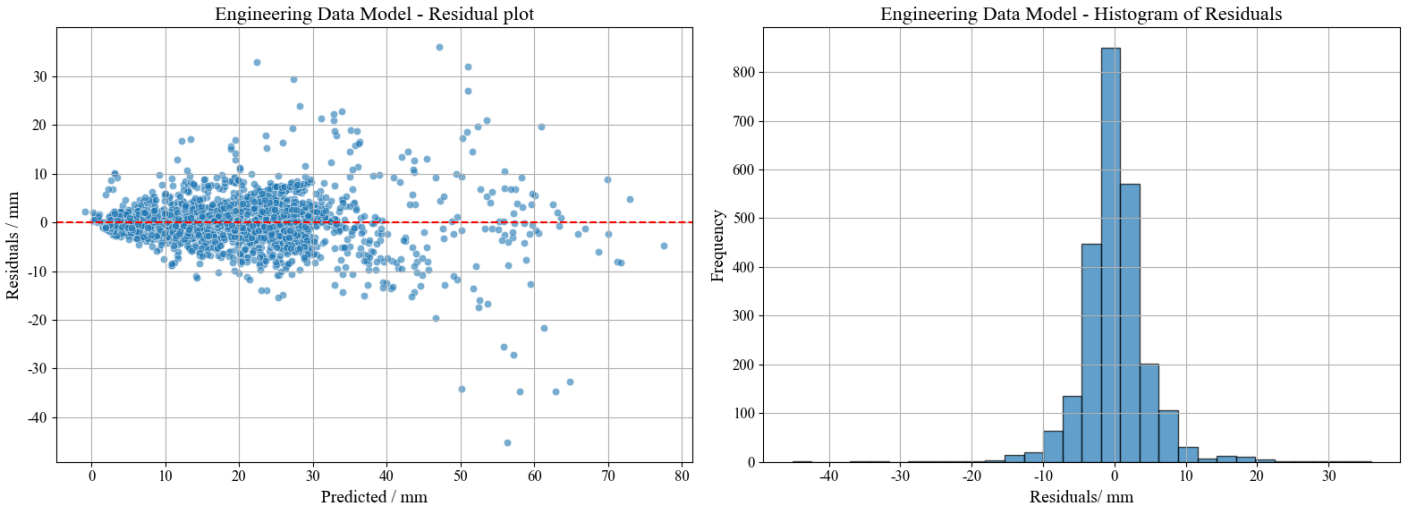

Figure 2: Schematic diagram of the internal structure of BPNN

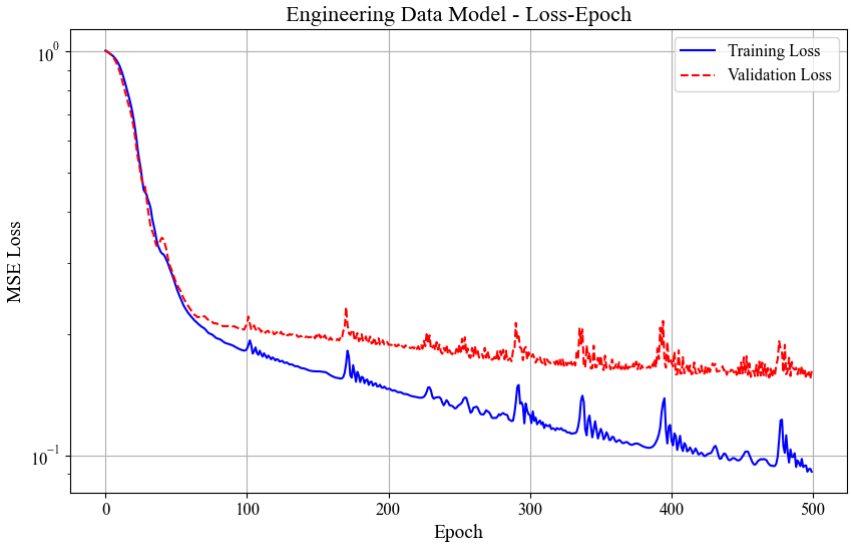

Figure 3: Schematic diagram of the internal structure of BPNN

In contrast, the model trained on the Finite Element (FE) dataset demonstrates superior performance, as shown in Fig. 4 and Fig. 5. The residuals are densely concentrated around the zero-error line, and the histogram forms a "tall and narrow" normal distribution. This excellent fit is quantified by an R^2 of 0.9811 ± 0.0017, signifying that most prediction errors are minimal and randomly distributed. The corresponding loss-epoch curve is exceptionally smooth; the minor oscillations observed in the later stages are an inherent characteristic of the iterative, gradient-based optimization algorithm as it performs fine-grained exploration near the optimal solution.

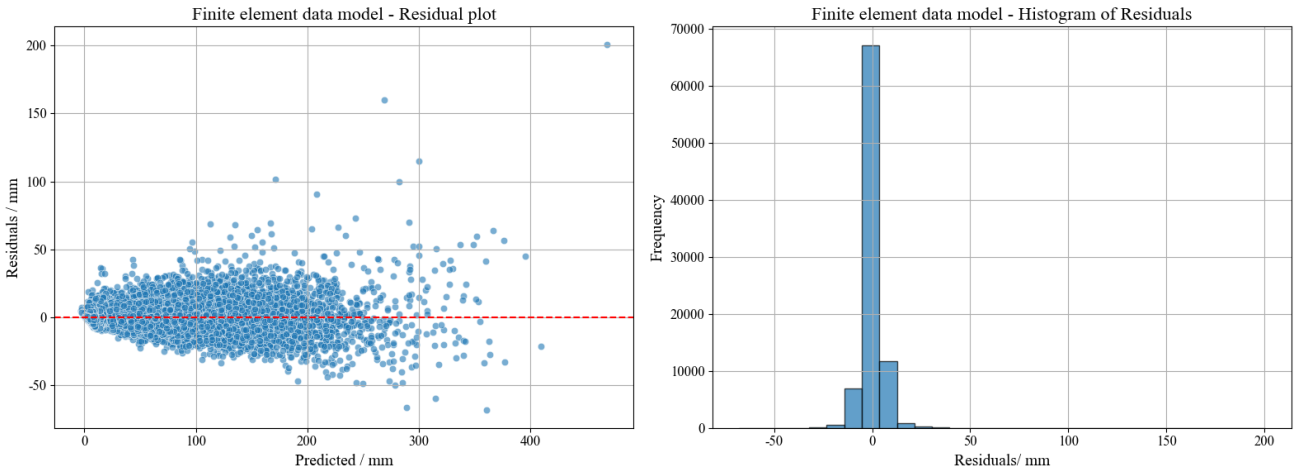

Figure 4: Schematic diagram of the internal structure of BPNN

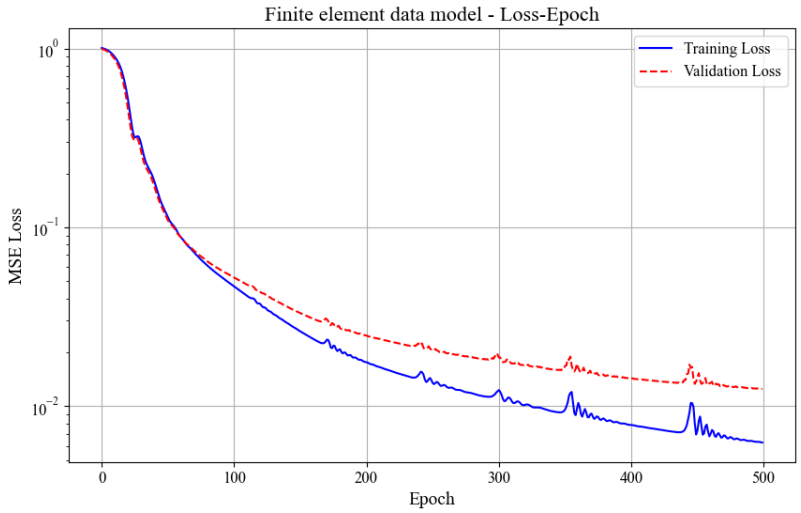

Figure 5: Schematic diagram of the internal structure of BPNN

Regarding the Fusion dataset, the results in Fig. 6 and Fig. 7 reveal a high degree of performance parity between the FE-only and the Fusion models. This is primarily attributed to a data dominance effect. The massive volume and comprehensive parametric coverage of the FE data saturated the model's learning capacity. The high-fidelity simulations, generated via automated PLAXIS, successfully encapsulated the fundamental physical behaviors of the geotechnical system. Consequently, the addition of the smaller engineering dataset, while representing real-world conditions, provided redundant information rather than novel, performance-enhancing insights.

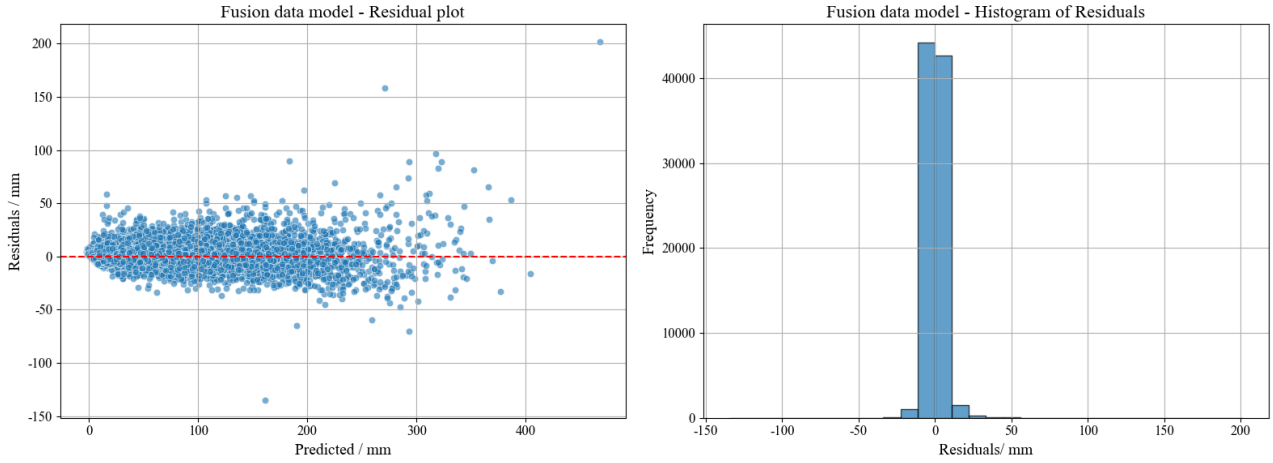

Figure 6: Schematic diagram of the internal structure of BPNN

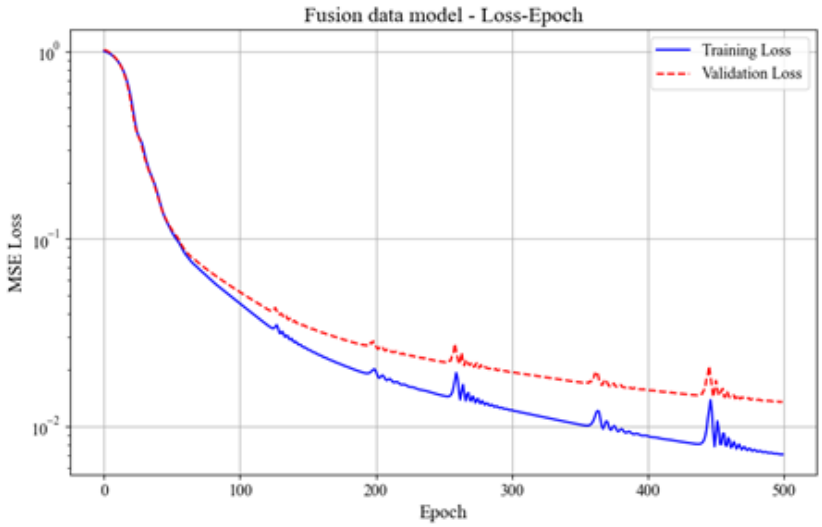

Figure 7: Schematic diagram of the internal structure of BPNN

3. RESULTS AND DISCUSSION

3.1 BPNN ON DIFFERENT DATASET

(1) Field Measurement dataset

By predicting 37 samples of engineering monitoring data, the results are shown in Figure 8. The absolute value of the error of the Engineering-sample model is mostly within 2 mm. The percentage of prediction results less than 2 mm is 73.53%, percentage of forecasts within 10% error is 79.4%. The maximum prediction result error is 6.96 mm, and the maximum error percentage is 60.72%. According to the experimental results, it is found that the prediction accuracy of the model based on the training of the engineering database is lower than that of the finite element database, and only partially meets the requirements of each excavation condition of the actual engineering pit.

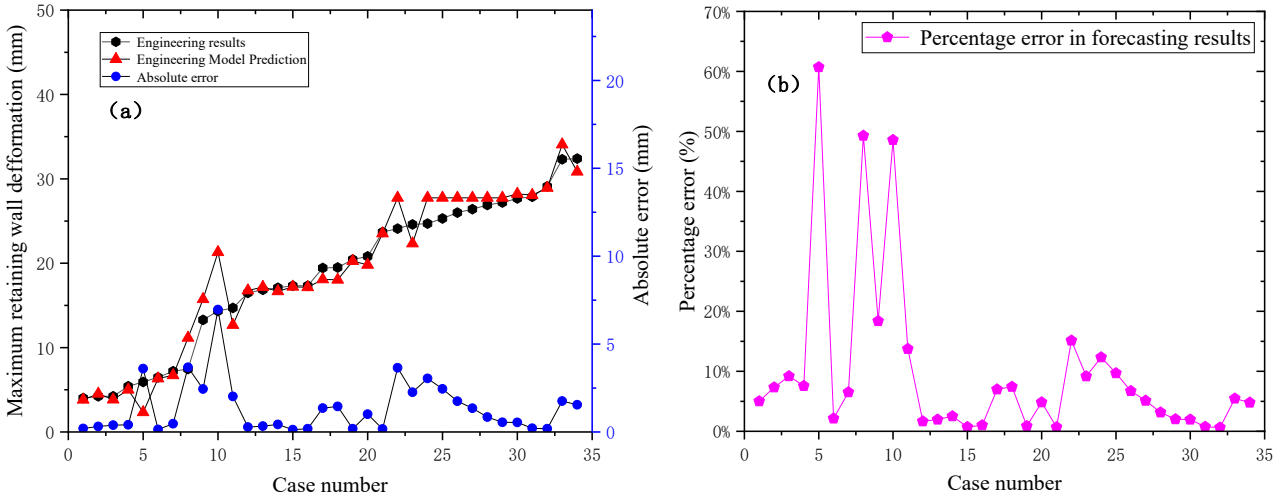

Figure 8. (a) Comparison of Engineering dataset prediction results; (b) Percentage error

(2) FEM dataset

The results of predicting 50 sets of randomly generated finite element cases are presented in Figure 9. The absolute value of the error of the FE-sample model is mostly within 2 mm, and the prediction accuracy is 2 mm. The percentage of prediction results less than 2 mm is 86%, percentage of forecasts within 10% error is 92%. The maximum prediction result error is 3.28 mm, and the maximum error percentage is 18.56%. Consequently, based on the training of the finite element database, the prediction accuracy of the model can meet the requirements for each excavation condition of the foundation pit generated by the finite element algorithms, and the majority of the prediction errors are less than 2 mm in absolute value.

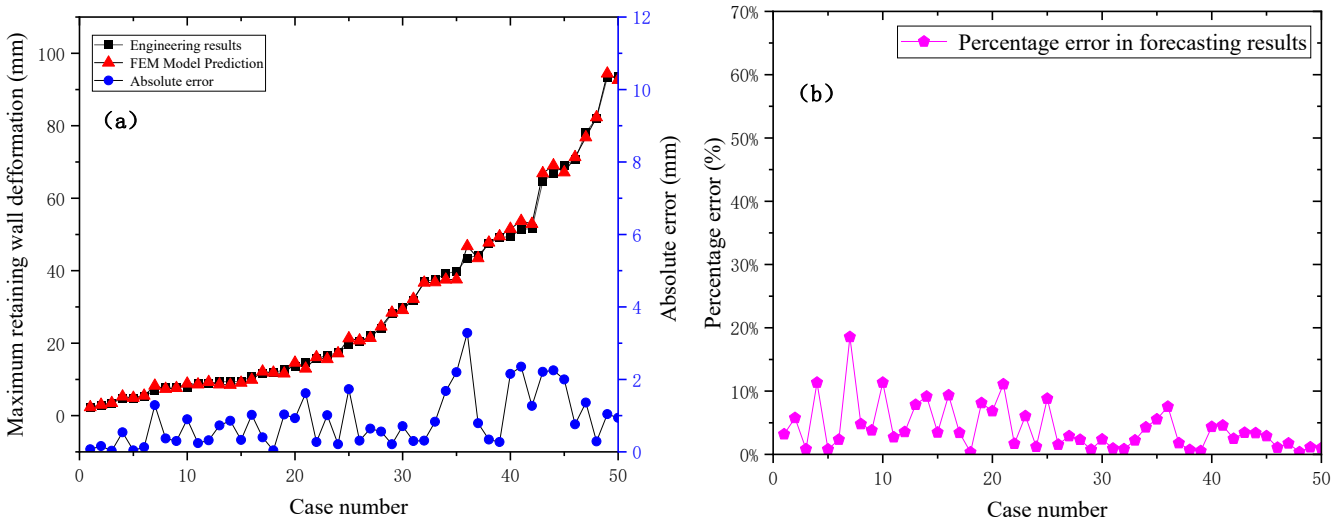

Figure 9. (a) Comparison of FEM dataset prediction results; (b) Percentage error

(3) Fused dataset

To validate the high fidelity of our large-scale finite element database and enhance the model's real-world applicability, we fused it with an engineering case history database. This hybrid approach aims to improve the model's generalization and robustness against atypical "edge cases" while establishing an extensible framework for a "living model" that can continuously evolve with new field data. Performance tests were subsequently conducted on this fused dataset.

The model's predictive performance was evaluated using 30 engineering and finite element cases not employed in training, with results shown in Figures 10. Prediction results based on the integrated database significantly outperformed those from the engineering database and were comparable to those from the finite element database. The mean absolute error was 0.782mm. Specifically, 96.77% of predictions had an absolute error of less than 2 mm, and 100% of predictions had a relative error within 5%. The maximum absolute error was 2.47 mm, corresponding to a maximum relative error of 4.33%.

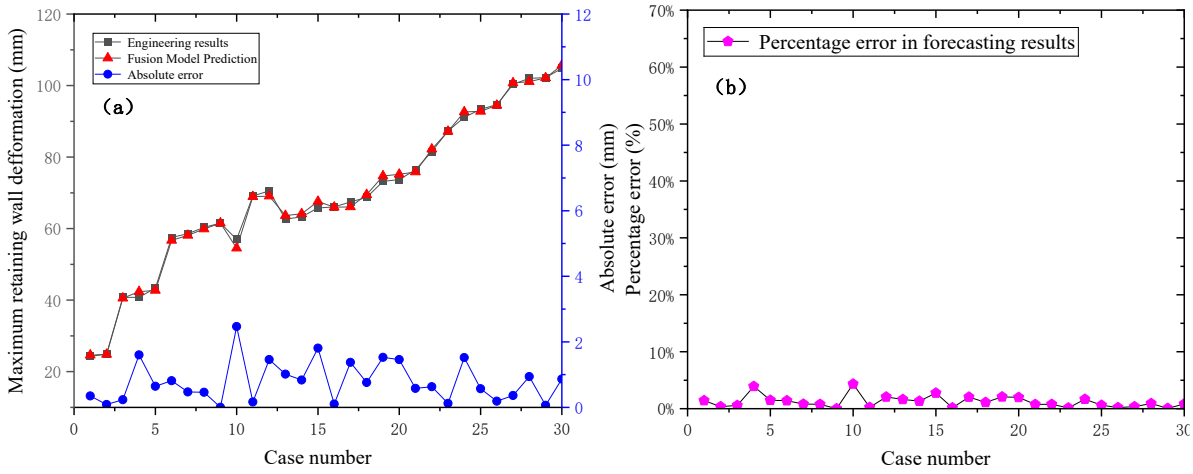

Figure 10. (a) Comparison of Fusion dataset prediction results; (b) Percentage error

3.2 ANALYSES AND DISCUSSION

To better compare model performance across different datasets, 40 real-world engineering datasets were selected for predictive analysis. Detailed comparative quantification is shown in Table 8. The Fusion dataset demonstrated optimal performance, with 97.5% of predictions exhibiting absolute errors below 2 mm and 100% showing relative errors under 5%, establishing its high reliability and precision. In contrast, while the Finite Element (FE) model also performed well (82.5% absolute error < 2mm), its higher maximum error of 3.97 mm revealed weaker generalization compared to the Fusion model's low 2.47 mm maximum error. The model trained solely on the Engineering dataset performed the worst, with severely inadequate accuracy (only 10% absolute error < 2mm) and a substantial maximum error of 5.48 mm, highlighting the limitations of relying on sparse, noisy field data.

Table 8. Comparison of Fusion dataset, FE dataset and Engineering dataset.

Comparison	Fusion dataset	FE dataset	Engineering dataset
Number of cases	90434	87368	3005
Number of prediction results（<2mm）	39(Total 40 groups)	33(Total 40 groups)	4(Total 40 groups)
Percentage of projected results（<2mm）	97.5%	82.5%	10%
Number of percentage error in forecasting results (<5%)	40(Total 40 groups)	38(Total 40 groups)	19(Total 40 groups)
Percentage of percentage error in forecasting results (<5%)	100%	95%	47.5%
Maximum absolute prediction error	2.47(mm)	3.97(mm)	5.48(mm)
Maximum percentage of prediction error	4.33%	6.26%	9.43%

This performance gap stems primarily from the fact that real engineering data contains noise, unmodeled physical uncertainties, and atypical edge cases not present in the extensive FE dataset. When the pure FE model encounters such parameters, its lack of relevant learning experience can lead to guesswork and significant errors. However, by integrating portions of the real engineering dataset, the hybrid model

learns the multi-coupling nature and uncertainty inherent in real-world phenomena, allowing it to outperform the pure finite element model in predicting real-world data.

4. CONCLUSION

This study generated a large-scale finite element (FE) database through extensive numerical modeling and compiled an engineering case database from field monitoring data. An analysis of models trained on these separate databases revealed their respective shortcomings. To address these limitations and improve predictive accuracy, a hybrid database was created by combining the FE and field data. A BPNN model trained on this hybrid database was then developed and validated against an independent engineering case. The primary conclusions are as follows:

(1) A reliable predictive model capable of overcoming the challenge of data scarcity was successfully developed. This study selected a comprehensive set of input parameters covering soil small-strain characteristics, excavation geometry, and retaining structure properties. Based on this, the model trained solely on the FE database already demonstrated high accuracy (with most absolute errors below 2 mm), validating the reasonableness of the parameter selection and the effectiveness of the model framework as a viable solution to address the problem of sparse field data.

(2) The hybrid database strategy significantly enhanced the model's prediction accuracy and generalization capability. By effectively fusing the parametric breadth of FE simulations with the real-world complexity captured in field data, the hybrid approach compensates for the deficiencies of single-source datasets. The model trained on the hybrid database exhibited superior performance, achieving a prediction accuracy on the test set where 96.77% of absolute errors were less than 2 mm and 100% of relative errors were less than 5%. Its accuracy and reliability were significantly better than models relying solely on FE or measured data.

LITERATURE

Bovolenta, R., Antonio, B. (2021), "Effect of deep excavations and deformable retaining structures on neighboring buildings: A case study". *Engineering Failure Analysis*, 122: 105269.

Borja, Ronaldo, I. (1990). "Analysis of Incremental Excavation Based on Critical State Theory". *Journal of Geotechnical Engineering*, 116(6), 964–985.

Burland, J.B. (1989), "Small is beautiful-The stiffness of soils at small strains". *Revue Canadienne De Géotechniqu*e, 26(4), 499–516.

Cao, J., Ding, W.Y., Zhao, D.S., Liu, H.M. (2014), "Time Series Forecast of Foundation Pit Deformation Based on BP Neural Network". *Applied Mechanics and Materials*, 556–562,5979–5983.

Clayton, C.R.I. (2011), "Stiffness at small strain: research and practice". *Géotechnique*, 61(1), 5–37.

Clough, G.W., Duncan, J.M. (1971), "Finite element analyses of retaining wall behavior". *Journal of Soil Mechanics & Foundation Engineering*, 97(12), 1657–1673.

Cui, D., Zhu, C., Li, Q., Huang, Q., Luo, Q. (2021), "Research on Deformation Prediction of Foundation Pit Based on PSO-GM-BP Model". *Advances in Civil Engineering*, 2021(1), 1–17.

Finno, R.J., Calvello, M. (2005). "Supported Excavations: Observational Method and Inverse Modeling". *Journal of Geotechnical & Geoenvironmental Engineering*, 131(7), 826–836.

Gao, G.Y., Huang, C., Sun, Y.M. (2002), "Application of GA-BP Neural Network in Excavation Monitoring of Deep Foundation Pit". *Underground Space*, 22(4),290-293+370.

Goh, A.T.C., Wong, K.S., Broms, B.B. (1995), "Estimation of lateral wall movements in braced excavations using neural networks". *Canadian Geotechnical Journal*, 32(6), 1059–1064.

Goh, A.T.C., Zhang, F., Zhang, W., Zhang, Y., Liu, H. (2017), "A simple estimation model for 3D braced excavation wall deflection". *Computers and Geotechnics*, 83,106–113.

Hsieh, P.G., Ou, C.Y. (1998), "Shape of ground surface settlement profiles caused by excavation". *Canadian Geotechnical Journal*, 35(6), 1004–1017.

Hu, Q.C., Hu, B., Jiang, H.F. (2013), "Application of BP Artificial Neural Network to the Displacement Prediction of Deep Foundation Pile". *Safety and Environmental Engineering*, 20(3), 154–158.

Jamali, A., Ghamati, M., Ahmadi, B., Nariman-Zadeh, N. (2013), "Probability of failure for uncertain control systems using neural networks and multi-objective uniform-diversity genetic algorithms (MUGA)". *Engineering Applications of Artificial Intelligence*, 26(2),714–723.

Kung, G.T., Juang, C.H., Hsiao, E.C., Hashash, Y.M. (2007), "Simplified Model for Wall Deflection and Ground-Surface Settlement Caused by Braced Excavation in Clays". *Journal of Geotechnical and Geoenvironmental Engineering*, 133(6),731–747.

Li, H., Wei, R., Zhu, H., Jia, C., Shi, G. (2021), "Numerical analysis of excavation stability of transfer station of Jinan Metro". *IOP Conference Series Earth and Environmental Science*, 632, 022019.

Lei, G., Gong, X. (2021), "Analysis of lateral displacement law of deep foundation pit support in soft soil based on improved MSD method". *Advances in Civil Engineering*, 2021, 1-15.

Ma, F. H., Yan, Z., Fan, Y. (2008), "Research on deformation prediction method of soft soil deep foundation pit". *Journal of Coalence and Engineering*, 14(4), 637–639.

Mana, A.I., Clough, G.W. (1981), "Prediction of movements for braced cuts in clay". *Geotechnical Special Publication*, 107(118): 1840–1858.

Mu, L., Chen, W., Huang, M., Lu, Q. (2020), "Hybrid Method for Predicting the Response of a Pile-Raft Foundation to Adjacent Braced Excavation". *International Journal of Geomechanics*, 20(4), 04020026.

Ou, C., Tang, Y. (1994), "Soil parameter determination for deep excavation analysis by optimization". *Journal of the Chinese Institute of Engineers*, 17(5), 671–688.

Peck, R.B. (1969), "Deep Excavations and Tunneling in Soft Ground". *Proc. of 7th ICSMFE*, *Mexico*.

Ren, D., Kang, C., Peng, T., Li, Y., & Wang, J. (2024), "Deformation Behavior of a Large-Scale Excavation and the Effect of an Adjacent Foundation Pit on the Excavation". *International Journal of Civil Engineering*, 1-13.

Whittle, A.J., Hashash, Y., Whitman, R.V. (1994), "Analysis of Deep Excavation in Boston". *Journal of Geotechnical Engineering*, 119(1), 69–90.

Xi, X., Li, A., Ban, J., Lu, W. (2010), "A neural network model for deformation prediction of deep foundation pit based on multivariate phase space reconstruction". *Sixth International Conference on Natural Computation.*

Xu, K.J., Poulos, H.G. (2000), "Theoretical Study of Pile Behaviour Induced by a Soil Cut". *International Society for Rock Mechanics*.

Yuan, J.R., Chi, Y.W., Liu, X.Z. (2000), "Dynamic Prediction on Displacement of Diaphragm Wall in Deep Foundation Excavation Engineering Using Artificial Neural Networks". *Journal of Tongji University*, 28(3), 282–286.

Zhang, J.Q., Qin, Y.J., Xie, L.F. (2020), "Predicting the settlement of Urumqi subway based on wavelet denoising and BP neural network". *IOP Conference Series: Earth and Environmental Science*, 570(5), 052019.

Zhang, R., Zheng, J., Pu, H., Zhang, L. (2011), "Analysis of excavation-induced responses of loaded pile foundations considering unloading effect". *Tunnelling and Underground Space Technology*, 26 (2),320–335.

Zeng, C. F., Zheng, G., Zhou, X. F., Xue, X. L., & Zhou, H. Z. (2019), "Behaviours of wall and soil during pre-excavation dewatering under different foundation pit widths". *Computers and Geotechnics*, *115*, 103169.

Seo, S., Chung, M. (2023), "Development of an Ensemble Prediction Model for Lateral Deformation of Retaining Wall Under Construction". *Journal of the Korean Geotechnical Society*, 39(4): 5-17.

(Provide contacts for author/s at the end of the paper, separated from References by one empty row.)

L. L. Mu

Department of Geotechnical Engineering, Tongji University, Shanghai 200092, China

mulinlong@tongji.edu.cn

K. Yan

Key Laboratory of Geotechnical and Underground Engineering of Ministry of Education, Tongji University, Shanghai 200092, China

E-mail address: